Materials Science Forum
ISSN: 1662-9752, Vol. 1034, pp 207-218
doi:10.4028/www.scientific.net/MSF.1034.207

Submitted: 2020-10-07
Revised: 2021-01-06
Accepted: 2021-01-27
Online: 2021-06-15

Optimization of Normal and Submerged FSP Parameters for Dissimilar Aluminium Joints Using Taguchi Technique

Velaphi Msomi[1,a*], Sipokazi Mabuwa[1,b]

[1]Cape Peninsula University of Technology, Faculty of Engineering and the Built Environment, Mechanical Engineering Department, P.O. Box 1906, Bellville, 7535, South Africa.

[a]msomiv@cput.ac.za, [b]mabuwas@cput.ac.za

Keywords: Taguchi, analysis of variance, friction stir processing, ultimate tensile strength, microhardness.

Abstract. The quality of the friction stir processed (FSPed) depends on the proper combination of processing parameters. The proper combination can only be found when a series of experiments have been conducted. However, the Taguchi technique was developed as a way of reducing numerous experiments that are time-consuming and costly. This paper reports on the optimization of parameters for the FSP that is conducted underwater (SFSP) and room temperature (NFSP). The Taguchi L18 method was employed in the design of experiments. The four factors used for the analysis had three factors with three-levels and one with two levels. The parameter combinations for SFSP were different from the combination found for NFSP. The level of parameter sensitivity was found to be influenced by the processing condition.

Introduction

Friction stir processing (FSP) is considered as the newly discovered solid-state technique that is used to enhance the performance of metals [1-3]. FSP was derived from friction stir welding (FSW) hence it uses the same principles similar to FSW. However, FSP differs from FSW on the principle that FSW works with two pieces while FSP works with only one piece or surface [4-7]. FSP technique can be used as a method of fabricating surface composites and also as the method of enhancing the properties of the material [8-11]. The fabrication of surface composites involves the inclusion of particles during the performance of processing [12-16]. FSP technique operates with specific combinations of parameters and each parameter has its impact on the behavior of the processed surface. Abrahams et al. (17) have investigated the optimum tool design to perform FSP on the AA7075-T651. The optimization of the tool profile was performed on AA5005-H34 and the optimized tool profile was then used to investigate the influence of rotational speed and traverse speed on the microstructure of the processed surface. The traverse speed was found to have more impact than rotational speed on the microhardness and mechanical properties of the processed surface.

The influence of the traverse speed and rotational speed on the performance of the AA6063 was investigated by Zhao et al. (18). The speed variation was performed in reference to the number of FSP passes. It was discovered that the grain size at low rotational speed was large compared to the high speed. It was further observed that there was grain size irregularity on the face and root surface of the stir zone. It was further observed that the grain size of the two-pass was larger compared to the single stir zone. The ultimate tensile strength was found to be lower than that of the base material at a low rotational but become higher at a higher rotational speed. John et al. (2019) have performed an investigation on the influence of pin profile on the friction stir processed AA2024-T351. The influence of pin profiles was studied with various combinations of rotational speed and traverse speed. The tool with a triangular profile was found to be the best tool in enhancing the mechanical properties of AA2024-T351.

Vignesh & Padmanaban (20) have studied the influence of tool rotational speed, traverse speed, and the tool shoulder on the wear resistance of the friction stir processed AA5083. The wear resistance of the processed plate was found to be better compared to the unprocessed plate. The contribution of each FSP parameter to the wear resistance of the processed plate yielded the development of the mathematical model that can be used to predict the wear resistance of the plate using various combinations of FSP parameters. The contribution of the number of FSP passes to the corrosion resistance of the hypereutectic Al-30Si alloy was studied by Rao et al. (21). A clear relationship between the grain size and the number of FSP passes was observed. The corrosion resistance was found to improving with the increase in the number of FSP passes. The grain refinement was also found to be increased with the number of FSP passes. Tangarasu et al. (22) have investigated the influence of the FSP traverse speed on the microstructure and mechanical properties of AA6082-TiC surface composite. The increase in traverse speed yielded the poor distribution of TiC particles on the processed surface. It was also discovered the increase in traverse speed led to an increase in the microhardness of the surface composite. It was further discovered that the increase in traverse resulted in a decrease in the wear rate of the surface composite.

One can see that the current cited literature dealt with parametric optimization through a few experiments. This however leaves a question of 'what would be the material's response when the number of experiments is increased?'. This question could be difficult to answer experimentally as it requires more resources. However, the statistical technique developed by Taguchi becomes handy in answering questions of this nature. This technique has been used by various researchers in optimizing parameters for experiments. This includes the optimization of friction stir welding parameters (similar and dissimilar materials) and friction stir processing parameters [23-29]. However, the focus will be on the application of this statistical technique in optimizing the FSP parameters.

Murthy et al. (30) have performed the optimization of FSP parameters and their significance towards the fabrication of the surface composite of AA7075-T651. The optimization was performed through the use of a statistical method called Taguchi. The parameters that were optimized included tool rotational speed, traverse speed, and the diameter of the hole that is used to fill the reinforcement. The sensitivity of each parameter towards the tensile strength of the composite was investigated through the use of analysis of variance (ANOVA). The tool rotational speed was found to have a significant contribution to the tensile strength of the composite. Sahu & Pal (31) employed the Taguchi grey relational analysis (GRA) technique in optimizing the FSP parameters on AM20 magnesium alloy. The welding speed, rotational speed, plunging depth, and shoulder diameter were the parameters chosen to be optimized as they play a major role in the performance of the processed surface. The L_{18} technique was employed in designing the experiments. The percentage method based on the ANOVA was used in ranking the influence of each parameter on the quality of the processed surface.

Ahmadkhaniha et al. (32) also employed the Taguchi technique in analyzing the most influential FSP parameter on the microhardness of the processed pure magnesium. The tilt angle, rotational speed, traverse speed, and penetration depth were the parameters chosen for optimization. The L_9 technique was employed in the design of experiments. The specific values of the selected parameters were found to the optimum values for the enhanced microhardness of the processed surface. The traverse speed, rotational speed, and the tilt angle of the tool were found to have a significant role in the microhardness of the process surface.

The few cited literature has revealed that the Taguchi technique can be used to optimize the FSW or FSP parameters with few experimental results. The technique is also capable of giving the relations of parameters and their contribution to the performance of the welded joint and the processed surface. It was observed that the majority of works employed the Taguchi technique in optimizing the FSP parameters for a single plate. There is no trace of works reporting on the employment of this technique for the optimization of the FSP parameters for processing friction stir welded dissimilar joints hence the aim of this paper. This paper reports on the employment of the Taguchi technique in optimizing the FSP parameters that are performed at room temperature and underwater. The tool tilt angle, tool rotational speed, traverse speed, and material positioning are the parameters that were chosen to be optimized as they play a significant role in the quality of the processed joint.

Experimental Procedure

The 6 mm thick 6083-T651 and 8011-H14 aluminum alloys (AA6083/AA8011) were cut into 250 x 70 mm in preparation for friction stir welding (FSW). The friction stir welded dissimilar

AA6083/AA8011 joints were produced using the rotational speed of 1100 rpm, traverse speed of 60 mm/min, and the tool tilt angle of 2º. The chemical composition of the materials used in this study is presented in Table 1. The tool used for FSW and FSP was made with high-speed steel (AISI4140) and its shoulder diameter was 20 mm, a triangular pin length of 5.8 mm, and a pin diameter of 6mm. The FSP was performed under two different conditions i.e. room temperature and underwater (submerged).

Table 1. Chemical compositions [33-35].

	Mg	Zn	Ti	Cr	Si	Mn	Fe	Cu	Al
AA8011-H14	0.28	0.084	0.016	0.028	0.52	0.46	0.74	0.13	Bal
AA6082-T6	1.1	0.2	-	0.25	0.9	0.7	0.5	0.1	Bal

The tensile test specimens were prepared and performed based on the ASTM-E8M-04 standard. The Vicker's microhardness test machine was used to perform microhardness tests with the guidance of the ASTM-E384 standard. The 300 g load was applied for 15 s in performing microhardness tests. Table 2 presents four parameters considered for this investigation and their associated levels. It should be noted that these parameters were employed in processing the dissimilar joint at room temperature and underwater.

Table 2. Processing parameters with their levels.

*MP	*RS	*TS	*TA	level
*8AS	600 rpm	40 mm/min	1 º	1
*6AS	900 rpm	70 mm/min	2 º	2
-	1200 rpm	100 mm/min	3 º	3

*8AS – AA8011-14 was positioned on the advancing side; 6AS – AA6083-T651 was positioned on the advancing side; RS – rotational speed; TS – traverse speed; TA – tilt angle; MP – material positioning

The Taguchi L_{18} factorial design was employed to minimize the number of experimental runs and the design matrix is presented in Table 3. This design matrix was produced through the use of MINITAB18 software.

Table 3. Taguchi L_{18} design matrix.

No.	MP	RS(rpm)	TS(mm/min)	TA(º)
1	8AS	600	40	1
2	8AS	600	70	2
3	8AS	600	100	3
4	8AS	900	40	1
5	8AS	900	70	2
6	8AS	900	100	3
7	8AS	1200	40	2
8	8AS	1200	70	3
9	8AS	1200	100	1
10	6AS	600	40	3
11	6AS	600	70	1
12	6AS	600	100	2
13	6AS	900	40	2
14	6AS	900	70	3
15	6AS	900	100	1
16	6AS	1200	40	3
17	6AS	1200	70	1
18	6AS	1200	100	2

Results and Discussions

The optimization of FSP parameters was performed for two different processing conditions i.e. room temperature (NFSP) and underwater (SFSP). The presentation of data analysis is arranged in this order for the whole paper.

Signal to noise ratio analysis

The optimization of FSP parameters was performed by analyzing the ultimate tensile strength (UTS), percentage elongation, and the microhardness of the processed AA8011/AA6082 dissimilar joint. The impact of each parameter on the response factors was analyzed through the use of the signal to noise ratio (SN) and the criteria used was the larger-the-better. This simply suggests that we are looking for the parameter combinations that will maximize the UTS, percentage elongation, and the microhardness of the joint processed under room temperature and underwater. The larger-the-better criteria can be calculated based on the following formula [32]:

$$S/N = -10\log\left(\frac{1}{n}\sum_{i=1}^{3}\frac{1}{y^2}\right) \quad (1)$$

where n is the repetition of experiments, y is the response factor which was UTS, percentage elongation, and microhardness in this study. Table 4 presents the SN ratio for parameter combinations for FSP performed at room temperature while Table 5 depicts the SN ratio for FSP performed underwater and their graphical representations are shown in Fig. 1 & 2.

Table 4. NFSP experimental results with relevant SN ratio.

MP	RS(rpm)	TS(mm/min)	TA(°)	UTS(MPa)	PE(%)	MH($HV_{0.3}$)	SNRA1	SNRA2	SNRA3
8AS	600	40	1	50.7	16.09	46.82	28.04	24.13	33.41
8AS	600	70	2	48.1	10.94	52.97	25.16	20.78	34.48
8AS	600	100	3	50.7	7.06	45.81	21.56	16.98	33.22
8AS	900	40	1	43.1	22.57	46.67	30.06	27.07	33.38
8AS	900	70	2	43.7	16.97	53.12	28.39	24.59	34.50
8AS	900	100	3	43.1	6.54	42.82	20.89	16.31	32.63
8AS	1200	40	2	45.3	25.00	44.42	30.63	27.96	32.95
8AS	1200	70	3	43.6	14.54	56.29	27.31	23.25	35.01
8AS	1200	100	1	45.3	9.69	39.95	24.07	19.73	32.03
6AS	600	40	3	72.2	13.74	43.49	26.98	22.76	32.77
6AS	600	70	1	75.1	12.43	46.05	26.25	21.89	33.27
6AS	600	100	2	87.2	14.91	41.52	27.60	23.47	32.36
6AS	900	40	2	56.1	10.43	45.23	24.77	20.37	33.11
6AS	900	70	3	75.4	11.09	45.08	25.33	20.90	33.08
6AS	900	100	1	87.8	20.43	38.77	29.73	26.21	31.77
6AS	1200	40	3	84.4	15.34	45.83	27.90	23.72	33.22
6AS	1200	70	1	77.5	7.37	45.55	21.97	17.35	33.17
6AS	1200	100	2	87.4	20.69	42.27	29.96	26.32	32.52

Table 5. SFSP experimental results with relevant SN ratio.

MP	RS(rpm)	TS(mm/min)	TA(°)	UTS(MPa)	PE(%)	MH($HV_{0.3}$)	SNRA1	SNRA2	SNRA3
8AS	600	40	1	28.0	6.23	65.57	28.94	15.89	36.33
8AS	600	70	2	46.9	6.02	51.25	33.42	15.59	34.19
8AS	600	100	3	53.9	14.86	40.22	34.63	23.44	32.09
8AS	900	40	1	21.7	4.14	59.70	26.73	12.34	35.52
8AS	900	70	2	55.8	8.43	52.46	34.93	18.52	34.40
8AS	900	100	3	69.4	21.46	40.61	36.83	26.63	32.17
8AS	1200	40	2	36.4	7.28	59.85	31.22	17.24	35.54
8AS	1200	70	3	36.8	4.71	53.16	31.32	13.46	34.51
8AS	1200	100	1	67.1	12.17	39.59	36.54	21.71	31.95
6AS	600	40	3	82.8	16.57	50.49	38.36	24.39	34.06
6AS	600	70	1	71.2	15.66	41.15	37.05	23.90	32.29
6AS	600	100	2	71.9	10.83	43.52	37.14	20.69	32.77
6AS	900	40	2	93.2	24.90	46.23	39.39	27.92	33.30
6AS	900	70	3	75.0	13.51	42.93	37.50	22.61	32.66
6AS	900	100	1	84.4	12.94	44.18	38.53	22.24	32.90
6AS	1200	40	3	86.5	23.31	47.37	38.74	27.35	33.51
6AS	1200	70	1	79.1	15.71	44.33	37.96	23.92	32.93
6AS	1200	100	2	77.4	14.54	44.55	37.78	23.25	32.98

Fig. 1. NFSP SN ratio plot (a) Ultimate tensile strength; (b) Percentage elongation; (c) Microhardness.

Fig. 1 (a) shows that the maximum UTS for the AA8011/AA6082 dissimilar joint processed under room temperature can be obtained when the material positioning is to level 2, the rotational speed is set to level 3, traverse speed is set to level 1 and the tilt angle is set to level 2. The same UTS parameter combination could yield maximum elongation (see figure 1(b)) [24]. For the maximum microhardness, the material positioning should be set at level 1, rotational speed at level 1, traverse speed be set at level 2 and the tilt angle be set to level 2. The maximum UTS for the joint processed underwater can be achieved when the material positioning is set to level 2, rotational speed set to level 2, traverse speed and tilt angle are both set to level 3 (see figure 2(a)). The parameter combination used for UTS can also be utilized for the achievement of maximum percentage elongation and this behavior is similar to the observed in NFSP. Figure 2(c) reveals that the maximum microhardness can be attained when material positioning is set to level 1, rotational speed set to level 1, traverse speed set to level 1, and the tilt angle set to level 2.

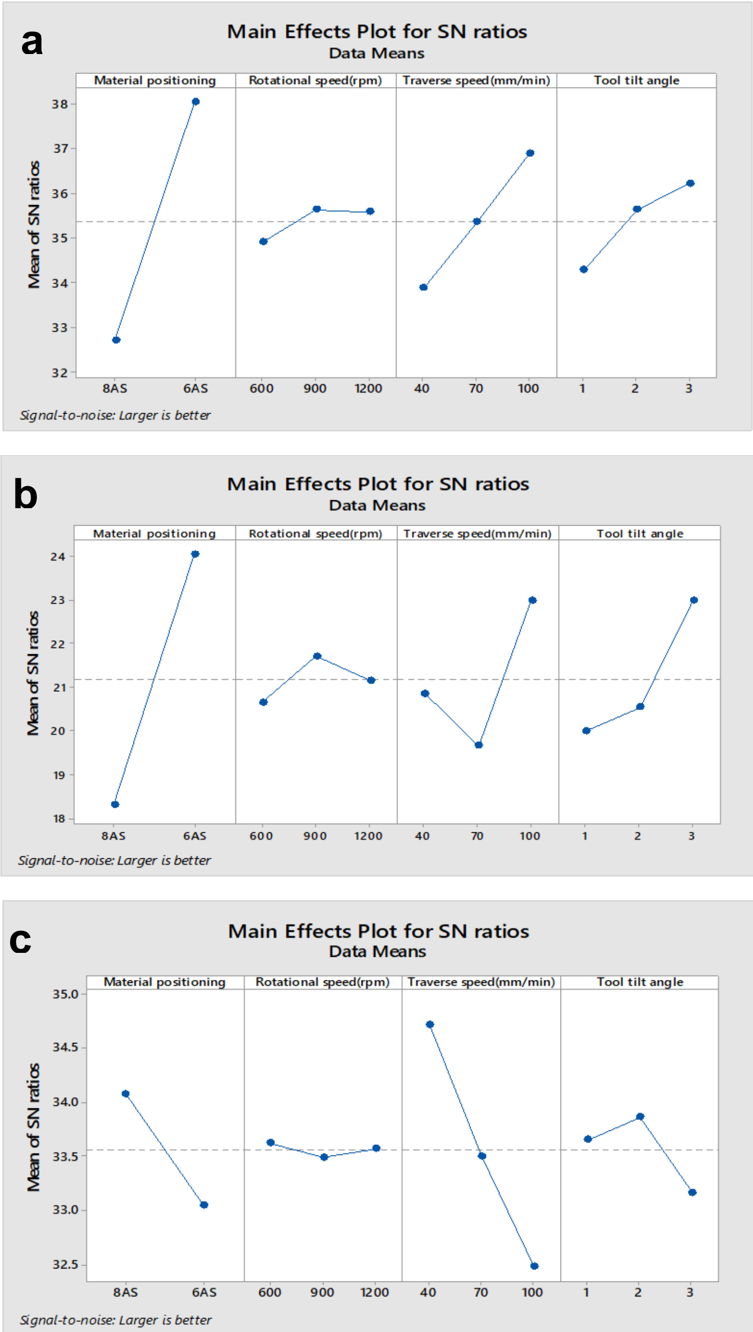

Fig. 2. SFSP SN ratio plot (a) Ultimate tensile strength; (b) Percentage elongation; (c) Microhardness.

Analysis of variance experimental data for NFSP

Ranking of contributing factors

It is crucial to analyze the influencing factor to each response factor of the dissimilar joint processed under room temperature. MINITAB18 software uses the delta ranking system to show the most critical factor to the response factor of the processed AA8011/AA6082 dissimilar joint. Table 6 shows that the UTS and percentage elongation for the NFSPed AA8011/AA6082 dissimilar joint is influenced by material positioning (rank 1), the rotational speed (rank 2), and traverse speed (rank 3) [36]. The percentage elongation according to Table 7 is influenced by traverse speed (rank 1), tilt angle (rank 2), rotational speed (rank 3), and material positioning (rank 4). Table 8 indicates that microhardness depends mostly on the traverse speed (rank 1), material positioning (rank 2), the tilt angle (rank 3), and rotational speed (rank 4).

Table 6. SN ration of parameters on ultimate tensile strength.

Level	MP	RS(rpm)	TS(mm/min)	TA(°)
1	26.23	25.93	28.06	26.69
2	26.72	26.53	25.73	27.75
3		26.97	25.64	24.99
Delta	2.76	2.43	1.04	0.49
Rank	1	2	3	4

Table 7.SN ratio of parameters on percentage elongation.

Level	MP	RS(rpm)	TS(mm/min)	TA(°)
1	22.31	21.67	24.33	22.73
2	22.55	22.57	21.46	23.91
3		23.05	21.50	20.65
Delta	0.24	1.39	3.26	2.87
Rank	4	3	1	2

Table 8. SN ratio of parameters on microhardness.

Level	MP	RS(rpm)	TS(mm/min)	TA(°)
1	33.51	33.25	33.14	32.84
2	32.81	33.08	33.92	33.32
3		33.15	32.42	33.32
Delta	0.71	0.17	1.50	0.48
Rank	2	4	1	3

Percentage of contribution factors

It is also better to analyze the contribution of each factor in terms of percentages and the probability of distribution (P-value). Table 9 shows that material positioning plays a major role in the variation of the UTS of the NFSPed AA8011/AA6082 dissimilar joint with a percentage of 87.95% followed by the rotational speed with 4.61%. This percentage contribution is in agreement with the rankings shown in Table 6. The percentage elongation (presented in Table 10) shows a strong dependency on the traverse speed and the tilt angle with 16.39% and 16.29%, respectively [31-34]. The F-value also agrees with the contribution percentage and both of these values concur with the ranking shown in Table 7. The traverse speed and the material positioning (see Table 11) play a significant role in the microhardness of the NFSPed AA8011/AA6082 dissimilar joint [34]. The F-value and the percentage contribution correlate with the ranking shown in Table 8.

Table 9. Factor contribution to the variation of ultimate tensile strength.

Source	DF	Contribution	F-Value
MP	1	87.95%	149.91
RS	2	4.61%	3.93
TS(mm/min)	2	1.26%	1.07
TA(°)	2	0.32%	0.27
Error	10	5.87%	
Total	17	100.00%	

Table 10. Analysis of Variance for percentage elongation.

Source	DF	Contribution	F-Value
MP	1	0.00%	0.00
RS(rpm)	2	4.15%	0.33
TS(mm/min)	2	16.39%	1.30
TA(°)	2	16.29%	1.29
Error	10	63.18%	
Total	17	100.00%	

Table 11. Analysis of Variance for microhardness.

Source	DF	Contribution	F-Value
MP	1	17.03%	11.74
RS(rpm)	2	1.19%	0.41
TS(mm/min)	2	58.94%	20.32
TA(°)	2	8.35%	2.88
Error	10	14.50%	
Total	17	100.00%	

Analysis of variance experimental data for SFSP

Ranking of contributing factors

The analysis performed on the room temperature was also performed on AA8011/AA6082 processed underwater. Table 12 shows that UTS for the SFSPed AA8011/AA6082 dissimilar joint is influenced by Material positioning (rank 1), the traverse speed (rank 2), rotational speed (rank 3) and tilt angle (rank 4). Percentage elongation (presented in Table 13) show strong dependency on material positioning (rank 1), tilt angle (rank 2), traverse speed (rank 3), and rotational speed (rank 4). Table 14 shows that the microhardness gets influenced by traverse speed (rank 1), material positioning (rank 2), tilt angle (rank 3), and rotational speed (rank 4) [28-30].

Table 12. SN ration of parameters on ultimate tensile strength.

Level	MP	RS(rpm)	TS(mm/min)	TA(°)
1	32.73	34.92	33.90	34.29
2	38.05	35.65	35.36	35.65
3		35.59	36.90	36.23
Delta	5.32	1.94	3.01	0.73
Rank	1	3	2	4

Table 13. SN ration of parameters on percentage elongation.

Level	MP	RS(rpm)	TS(mm/min)	TA(°)
1	18.31	20.65	20.86	20.00
2	24.03	21.71	19.67	20.54
3		21.16	22.99	22.98
Delta	5.72	1.06	2.98	3.33
Rank	1	4	3	2

Table 14. SN ration of parameters on microhardness.

Level	MP	RS(rpm)	TS(mm/min)	TA(°)
1	34.08	33.62	34.71	33.65
2	33.04	33.49	33.50	33.86
3		33.57	32.48	33.17
Delta	1.03	0.13	2.23	0.70
Rank	2	4	1	3

Percentage of contribution factors

Table 15 depicts that material positioning and traverse speed play a major role in the variation of SFSPed AA8011/AA6082 dissimilar joint and this percentage contribution correlate with the relevant F-value of these factors. The two major contributing factors agree with the rankings shown in Table 12. The variation of percentage elongation for SFSPed AA8011/AA6082 dissimilar joint depends on the material positioning and the tilt angle with a percentage contribution of 37.22% and 9.8%, respectively. This percentage contribution (see Table 16) correlates with the factor ranking shown in Table 13. The percentage contribution shown in Table 17 suggests that traverse speed and material positioning play a significant role in the microhardness of the SFSPed AA8011/AA6082 dissimilar joint [11,17-19]. This percentage contribution correlates with the rankings shown in Table 14.

Table 15. Factor contribution to the variation of UTS.

Source	DF	Contribution	F-Value
MP	1	70.94%	36.29
RS(rpm)	2	3.72%	0.95
TS(mm/min)	2	3.95%	1.01
TA(°)	2	1.84%	0.47
Error	10	19.55%	
Total	17	100.00%	

Table 16. Factor contribution to the variation of percentage elongation.

Source	DF	Contribution	F-Value
MP	1	37.22%	8.61
RS(rpm)	2	1.83%	0.21
TS(mm/min)	2	7.93%	0.92
TA(°)	2	9.80%	1.13
Error	10	43.23%	
Total	17	100.00%	

Table 17. Factor contribution to the variation of microhardness.

Source	DF	Contribution	F-Value
MP	1	14.23%	5.37
RS(rpm)	2	0.10%	0.02
TS(mm/min)	2	53.57%	10.11
TA(°)	2	5.60%	1.06
Error	10	26.49%	
Total	17	100.00%	

Conclusion

The parametric optimization for performing friction stir processing on the AA8011/AA6082 dissimilar joint was performed with the assistance of the Taguchi L_{18} factorial method. The optimization of parameters was based on conducting FSP under two different conditions i.e. room temperature and underwater. The Taguchi technique showed that the maximum UTS for NFSP could be attained when the rotational speed is set to level 3, traverse speed set to level 1, material positioning set to level 2, and the tilt angle set to level 2. The maximum percentage elongation for NFSP could be attained when the rotational speed is set to level 3, traverse speed set to level 3, material positioning set to level 2, and the tilt angle set to level 2. Lastly, the maximum microhardness for NFSP could be attained when the rotational speed is set to level 1, traverse speed set to level 2, material positioning set to level 1, and the tilt angle set to level 2. The maximum UTS for SFSP could be attained when the rotational speed is set to level 2, traverse speed set to level 3, material positioning set to level 2, and the tilt angle set to level 3. The maximum percentage elongation for SFSP could be attained when the rotational speed is set to level 3, traverse speed set to level 1, material positioning set to level 2, and the tilt angle set to level 3. Lastly, the maximum microhardness for NFSP could be attained when the rotational speed is set to level 1, traverse speed set to level 1, material positioning set to level 1, and the tilt angle set to level 2. The conditions through which the FSP has conducted influence the combination of parameters.

Acknowledgment

The authors would like to thank the National Research Foundation through the Thuthuka Grant instrument for financial support to the study.

References

[1] Mishra RS, Ma ZY, Charit I.(2003). Friction stir processing: a novel technique for fabrication of surface composite. Materials Science and Engineering: A 341(1–2), 307-310.

[2] Kurt A, Uygur I, Cete E.(2011). Surface modification of aluminium by friction stir processing. Journal of Materials Processing Technology 211(3), 313-317

[3] Borrego LP, Costa JD, Jesus JS, Loureiro AR, Ferreira JM.(2014). Fatigue life improvement by friction stir processing of 5083 aluminium alloy MIG butt welds. Theoretical and Applied Fracture Mechanics 70, 68-74.

[4] Vignesh RV, Padmanaban R.(2018). Intergranular corrosion susceptibility of friction stir processed aluminium alloy 5083. Materials Today: Proceedings 5(8), 16443-16452.

[5] Behnagh RA, Shen N, Abdollahi M, Ding H.(2016). Ultrafine-Grained Surface Layer Formation of Aluminum Alloy 5083 by Friction Stir Processing. Procedia CIRP 45, 243-246.

[6] Jesus JS, Costa JM, Loureiro A, Ferreira JM.(2017). Fatigue strength improvement of GMAW T-welds in AA 5083 by friction-stir processing. International Journal of Fatigue 97, 124-134

[7] Khan M, Rehman A, Aziz T, Shahzad M, Naveed K, Subhani T.(2018).Effect of inter-cavity spacing in friction stir processed Al 5083 composites containing carbon nanotubes and boron carbide particles. Journal of Materials Processing Technology 253, 72-85.

[8] Kurt HI.(2016). Influence of hybrid ratio and friction stir processing parameters on ultimate tensile strength of 5083 aluminum matrix hybrid composites. Composites Part B: Engineering 93, 26-34

[9] Liu P, Shi Q, Zhang Y.(2013). Microstructural evaluation and corrosion properties of aluminium matrix surface composite adding Al-based amorphous fabricated by friction stir processing. Composites Part B: Engineering 52, 137-143.

[10] Kianezhad M, Raouf AH.(2019). Effect of nano-Al2O3 particles and friction stir processing on 5083 TIG welding properties. Journal of Materials Processing Technology 263, 356-365.

[11] Huang GQ, Yan YF, Wu J, Shen YF, Gerlich AP.(2019). Microstructure and mechanical properties of fine-grained aluminum matrix composite reinforced with nitinol shape memory alloy particulates produced by underwater friction stir processing. Journal of Alloys and Compounds 786, 257-271.

[12] Azizieh M, Kokabi AH, Abachi P.(2011). Effect of rotational speed and probe profile on microstructure and hardness of AZ31/Al2O3 nanocomposites fabricated by friction stir processing. Materials & Design 32(4), 2034-2041

[13] Reddy KV, Naik RB, Rao GR, Reddy GM, Kumar RA.(2020). Microstructure and damping capacity of AA6061/graphite surface composites produced through friction stir processing. Composites Communications 20, 100352.

[14] Prabhu SM, Perumal EA, Arulvel S.(2020). Development of multi-pass processed AA6082/SiCp surface composite using friction stir processing and its mechanical and tribology characterization. Surface and Coatings Technology 394, 125900.

[15] Barati M, Abbasi M, Abedini M.(2019). The effects of friction stir processing and friction stir vibration processing on mechanical, wear and corrosion characteristics of Al6061/SiO2 surface composite. Journal of Manufacturing Processes 45, 491-497.

[16] Mehta KM, Badheka VJ.(2019). Wear behavior of boron-carbide reinforced aluminum surface composites fabricated by Friction Stir Processing. Wear 426–427(B), 975-980.

[17] Abrahams R, Mikhail J, Fasihi P.(2019). Effect of friction stir process parameters on the mechanical properties of 5005-H34 and 7075-T651 aluminium alloys. Materials Science and Engineering: A 751, 363-373

[18] Zhao H, Pan Q, Qin Q, Wu Y, Su X.(2019). Effect of the processing parameters of friction stir processing on the microstructure and mechanical properties of 6063 aluminum alloy. Materials Science and Engineering: A 751, 70-79.

[19] John J, Shanmughanatan SP, Kiran MB.(2018). Effect of tool geometry on microstructure and mechanical Properties of friction stir processed AA2024-T351 aluminium alloy. Materials Today: Proceedings 5(1), 2965-2979.

[20] Vignesh RV, Padmanaban R.(2018). Influence of friction stir processing parameters on the wear resistance of aluminium alloy AA5083. Materials Today: Proceedings 5(2), 7437-7446.

[21] Rao AG, Katkar VA, Gunasekaran G, Deshmukh VP, Prabhu N, Kashyap BP.(2014). Effect of multipass friction stir processing on corrosion resistance of hypereutectic Al–30Si alloy. Corrosion Science 83, 198-208.

[22] Thangarasu A, Murugan N, Dinaharan I, Vijay SJ.(2014). Influence of Traverse Speed on Microstructure and Mechanical Properties of AA6082-TiC Surface Composite Fabricated by Friction Stir Processing. Procedia Materials Science 5, 2115-2121

[23] Tutar M, Aydin H, Yuce C, Yavuz N, Bayram A.(2014). The optimisation of process parameters for friction stir spot-welded AA3003-H12 aluminium alloy using a Taguchi orthogonal array. Materials & Design 63, 789-797.

[24] Shunmugasundaram M, Kumar AP, Sankar LP, Sivasankar S.(2020). Optimization of process parameters of friction stir welded dissimilar AA6063 and AA5052 aluminum alloys by Taguchi technique. Materials Today: Proceedings 27(2), 871-876.

[25] Lakshminarayanan AK, Balasubramanian V.(2008). Process parameters optimization for friction stir welding of RDE-40 aluminium alloy using Taguchi technique. Transactions of Nonferrous Metals Society of China 18(3), 548-554

[26] Tutar M, Aydin H, Yuce C, Yavuz N, Bayram A.(2014). The optimisation of process parameters for friction stir spot-welded AA3003-H12 aluminium alloy using a Taguchi orthogonal array. Materials & Design 63, 789-797.

[27] Devaiah D, Kishore K, Laxminarayana P.(2018). Optimal FSW process parameters for dissimilar aluminium alloys (AA5083 and AA6061) Using Taguchi Technique. Materials Today: Proceedings 5(2), 4607-4614.

[28] Meena K, Kumar A, Pandya SN.(2017). Optimization of Friction Stir Processing Parameters for 60/40 Brass using Taguchi Method. Materials Today: Proceedings 4(2), 1978-1987.

[29] Rathee S, Maheshwari S, Siddiquee AN, Srivastava M, Sharma SK.(2016). Process parameters optimization for enhanced microhardness of AA 6061/ SiC surface composites fabricated via Friction Stir Processing (FSP). Materials Today: Proceedings 3(10), 4151-4156

[30] Murthy V, Kumar SD, Saju KK, Rajaprakash BM, Rajashekar R.(2019). Optimization of Friction Stir Processing parameters for manufacturing silicon carbide reinforced aluminum 7075-T651 surface composite. Materials Today: Proceedings 18(7), 4549-4555.

[31] Sahu PK, Pal S.(2015). Multi-response optimization of process parameters in friction stir welded AM20 magnesium alloy by Taguchi grey relational analysis. Journal of Magnesium and Alloys 3(1), 36-46.

[32] Ahmadkhaniha D, Sohi MH, Zarei-Hanzaki A, Bayazid SM, Saba M.(2015). Taguchi optimization of process parameters in friction stir processing of pure Mg. Journal of Magnesium and Alloys 3(2), 168-172.

[33] Mabuwa S, Msomi V.(2020). The effect of friction stir processing on the friction stir welded AA1050-H14 and AA6082-T6 joints. Materials Today: Proceedings 26(2), 193-199.

[34] Selvaraj G, Karthikeyan T, Mohanadass R, Indhumath S (2015). Investigation on mechanical properties of welded aluminium joints of aa 8011 using friction stir welding. International Journal of Applied Engineering Research 10(13): 11095-11100.

[35] Braga DFO, de Sousa LMC, Infante V, da Silva LFM, Moreira PMG (2016). Aluminium Friction Stir Weld-bonded Joints. The Journal of Adhesion 92(7-9): 665-678.

[36] Prakash JU, Sadhana AD, Ananth S, Pillai KVA. (2020). Optimization of wear parameters of aluminium matrix composites (LM6/Fly Ash) using Taguchi technique. Materials Today: Proceedings, In press.